

Natural etching rates of feldspar and hornblende

Dedicated to Paul W. Schindler on his retirement

Susan L. Brantley¹, Adam C. Blai¹, David L. Cremeens², Ian MacInnis¹ and Robert G. Darmody³

¹ Department of Geosciences, Pennsylvania State University, University Park, PA 16802, USA

² G. A. I. Consultants Inc., Monroeville, PA, USA

³ Dept. of Agronomy, Univ. of Illinois, Urbana, IL 61801, USA

Key words: Weathering rates, etch pits, mineral dissolution kinetics, mineral surfaces.

ABSTRACT

Analysis of the etch-pit size distributions (PSDs) observed on potassium feldspar and hornblende grains in a soil catena in loess (age = 12,500 y) reveals natural mineral etching rates. Rates estimated for hornblende (6 to 9×10^{-15} mol/m²s) are based on consistent crystallographically controlled etch pits, while rates estimated for potassium feldspar (2×10^{-15} mol/m²s) are based on irregularly shaped pits. Although little difference in etching rate is observed between soil horizons, the highest etching rates generally occur in the upper B horizons where pH values are lowest. Decreasing soil drainage correlates with an increase in pit density, n° , probably due to increased grain wetting, while decreased drainage correlates with a decrease in pit growth rate (G), probably due to increased dissolved solute concentrations. The PSD model predicts that etching rate is a function of n° and of G^4 . Etching rates calculated for potassium feldspar do not vary with drainage, while those of hornblende decrease with decreasing drainage. Estimated etching rates are lower than bulk dissolution rates measured in the laboratory.

Introduction

Significant progress has been made in applying the “surface complexation model” (e.g. Schindler and Stumm, 1992) to predict mineral dissolution kinetics measured in the laboratory. However, most estimates of mineral dissolution rates in natural systems are slower than rates measured in the laboratory. Brantley (1992) summarized 7 explanations for this discrepancy: lack of understanding of reaction mechanism, experimental error, differences in inhibitor concentrations and chemical affinity, inaccuracies in reactive surface area estimation, inaccuracies in wetted surface area estimation, temperature variability, and biological processes.

If (i) the distribution of wetted surface area or (ii) the concentration of inhibitors or (iii) the saturation index of soil waters are of primary importance determining natural mineral weathering rates, then etching of mineral grains should depend on soil depth (or horizon)

or soil drainage. However, most investigations of field dissolution rates have relied on mass balance arguments in watersheds (e.g. Paces, 1983; Velbel, 1993), soil plots (e.g. Swoboda-Colberg and Drever, 1993), and aquifers (e.g. Claasen and White, 1979; Rowe and Brantley, 1993) and have not distinguished between areas of full and partial saturation. Comparative studies of mineral etching *in situ* allow such an assessment. For example, Brantley et al. (1986) identified a distinct decrease in etching of quartz surfaces as a function of depth in a soil profile developed on the Parguaza granite in Venezuela, and attributed the lack of dislocation-etch pits to high silica concentrations in porewaters lower in the profile. Hall and Horn et al. (1993) observed that etching of hornblende in soils decreases rapidly with increasing soil depth, and that etching was faster where atmospheric precipitation was higher and where soil grains were coarser.

In this paper, we apply the pit-size distribution (PSD) model (MacInnis and Brantley, 1993) to an investigation of etching on soil grains of potassium feldspar and hornblende from a soil catena (Creameens et al. 1992). The catena consists of three soils of identical composition and grain size distribution, but varying by extent of drainage as determined from soil color patterns.

Formation of etch pits on hornblende and feldspar

The dynamics of etch pit nucleation and growth have been described (e.g. Brantley et al., 1986). For very small etch pits on perfect surface, the increase in free energy due to surface area increase outweighs the decrease in energy due to dissolution of a small volume. Only if the etch pit grows to the critical radius where a net decrease in energy is achieved, can the pit grow spontaneously (Brantley et al., 1986). For etch pits at dislocations, however, the strain energy allows pits to open spontaneously, unless the solute reaches the critical concentration, C_{crit} , above which dislocation etch pit growth is not expected:

$$C_{\text{crit}} = C_0 \exp\left(\frac{-2\pi^2 \gamma^2 V}{RT\tau b^2}\right) \quad (1)$$

Here, C_0 is the equilibrium solubility, γ is the interfacial energy, V is the molar volume, R is the gas constant, T is the absolute temperature, τ is the shear modulus, and b is the Burger's vector. When the concentration of dissolved solutes surpasses C_{crit} , dissolution stops at all but the highest energy sites, such as kinks and edges. For dissolution below this critical value, etching should occur extensively on the mineral surface, while above the critical value, we expect little or no pit nucleation, and slower growth (opening) of pits present on the surface. Brantley et al. (1986) suggested that dissolution rate should decrease rapidly above C_{crit} and showed evidence for this effect in dissolution of quartz.

PSD theory

The PSD model (MacInnis and Brantley, 1993) considers the population density of etch pits within a given size range during dissolution, and is based on models of crystal size distribution (Marsh, 1988). The pit size distribution depends on the number of pits per unit size per unit area, n ($\text{m}^{-1}\text{m}^{-2}$), and the growth rate, G (ms^{-1}), of pits growing into and out

of that size window. The rate of annihilation of pits, \dot{a} (s^{-1}), is the rate of coalescence of two pits together (net loss of one pit), or if the pit stops deepening, the rate at which the pit disappears as the flat surface of the crystal recedes.

Assuming that growth rate is time- and size-independent at constant temperature, then we can write a population balance on pits and derive the steady-state pit size distribution equation where $\frac{\partial n}{\partial t} = 0$ and where n^0 is defined as the density of etch pits at time t_0 :

$$n = n^0 \exp\left(-\frac{W}{G\tau}\right) \quad (2)$$

For these assumptions, a plot of $\ln(n)$ against W should produce a straight line with slope $-1/G\tau$ and intercept $\ln(n^0)$. We define τ as the reciprocal of the annihilation rate, or the mean lifetime of a pit. The rate of pit nucleation, J , is defined as Gn^0 (Marsh, 1988).

A linear PSD plot ($\ln(n)$ vs. W) results when there is a balance between nucleation and annihilation of pits, and where there is size- and time-independent growth rate of pits. At steady state, PSD coefficients do not change with time. However, linear PSDs are also possible for non-steady-state systems (Marsh 1988). Kerrick et al. (1991) have argued that the CSD model is inappropriate for some cases: however, their criticisms are not applicable to the pit model because etch pits are removed from the dissolving mineral surface by coalescence or simply by growth stoppage and annihilation by surface recession (MacInnis and Brantley, 1993).

Where coalescence is the operative model of annihilation, the smallest pits will be removed from the population, and the PSD may become "humped". Kerrick et al. (1991) and MacInnis and Brantley (1993) have shown that humped CSD and PSD plots can also result from a variation in nucleation rate with time where no annihilation is occurring.

The contribution to the bulk dissolution rate from a single etch pit depends on the width, W , pit wall slope, θ , and the geometry of the pit. The contribution of etch pits to the bulk dissolution rate, $R_{\text{pit}}(W)$, depends on the number density, $n(W)$, and the rate of dissolution of each pit:

$$R_{\text{pit}}(W) = \int_0^{\infty} f(W) n^0 \exp\left(-\frac{W}{G\tau}\right) dW \quad (3)$$

where $f(W)$ is the geometric function describing the rate of growth of one pit. For pit geometries of right-pyramids, we can define $f(W)$ (MacInnis and Brantley, 1993):

$$f(W) = W^2 \frac{v_x \tan \theta}{V} \quad (4)$$

where v_x is the half-width opening rate ($= 0.5 G$). Using this value of $f(W)$, equation (3) yields:

$$R_{\text{pit}} = \frac{2n^0 v_x \tan \theta}{V} (G\tau)^3 \quad (5)$$

As pointed out by MacInnis and Brantley (1993), $G\tau$ represents the average pit width of the distribution; Equation 5 thus describes the rate of dissolution (growth) of the average

pit, integrated over all pits (the etching rate). Given that $v_x = 0.5 G$, Equation 5 shows that $R_{\text{pit}}(W)$ is a function of n^0 and G^4 .

Soil samples and data collection

Soil grains from three forested loessal soil profiles were analyzed by Cremeens et al. (1992). The three soils comprise a catena: the well-drained Fayette soil is only rarely saturated, the somewhat poorly drained Stronghurst soil is saturated for significant periods, and the poorly drained Traer soil is saturated most of the time (Bouma, 1983). Drainage was determined using standard techniques of analysis of soil color patterns (Cremeens, et al. 1992). The loess, located in Adams County Illinois, ranges in thickness from 3.0 to 7.5 m, and overlies 6 to 11 m of till of Illinoian to pre-Illinoian age. The soil age is $12,500 \pm 500$ y. Soil pH is low for all three soils, and minimum pH occurs in the upper B

Table 1. Distribution of etch pit diameters

Diameter μm	Fayette BE	Fayette Bt	Fayette C	Strong. E	Strong. Bt	Strong. Cg	Traer E	Traer Btg	Traer Cg
<i>potassium feldspar</i>									
0.2	231	70	12	445	107	243	803	1576	148
0.6	1564	1078	560	2225	2017	1135	2863	3430	1684
1.0	972	992	491	1041	1543	679	1177	1641	1069
1.4	389	442	190	436	467	316	385	481	566
1.8	143	234	86	150	168	129	135	188	191
2.2	68	71	39	72	79	56	47	61	58
2.6	39	45	13	22	25	29	18	32	19
3.0	14	15	9	12	9	12	4	8	9
3.4	13	4	6	5	6	6	*1	4	2
3.8	6	3	2	1	1	2	*2	*1	*1
4.2	1	1	1	1	1	1	*3	*1	*1
4.6	*2	*0	*1	*3	*2	*0	*1	*1	*1
5.0	*6	*0	*3	*2	*1	*0	*1	*1	*1
<i>hornblende</i>									
0.2	*0	*97	*34	*95	*28	*13	*174	*15	*87
0.6	249	995	709	1039	647	478	2357	1802	1996
1.0	1153	1557	1344	1703	1578	1185	2728	2960	2577
1.4	1193	1284	879	1256	1055	890	1228	1295	1300
1.8	823	740	476	666	595	543	472	661	568
2.2	505	409	267	332	387	189	227	309	220
2.6	254	210	162	142	197	116	100	118	121
3.0	146	122	106	91	101	52	66	*152	47
3.4	68	76	70	23	60	46	35	*132	26
3.8	43	50	31	21	35	19	23	*113	19
4.2	28	25	39	10	15	7	*16	*77	*5
4.6	11	19	19	8	7	3	*13	*28	*4
5.0	*22	*66	*61	*14	*25	*19	*27	*104	*8

* not used in PSD regression (Fig. 2)

horizon. The suffix *t* in tables and figures refers to zones of visible clay accumulation, and the suffix *g* indicates dull grey color resulting from reduction caused by impeded drainage (gley).

Creameens et al. (1992) sampled the 53–100 μm size fraction of three horizons from each profile. Samples from three horizons in each soil type were picked from cleaned mineral separates, mounted and Au-Pd coated. Minerals were identified using optical and scanning electron microscopy fitted with EDX analysis.

Creameens et al. (1992) recorded the total number of pits from a horizon sample in addition to the number of pits per size fraction based on visual and digital analysis of SEM micro-photography (Table 1). Etch pits were defined as closed perimeter depressions on that portion of the grain surface enclosed by the grain perimeter. Data is summarized as number of pits observed per 20 grains. The equivalent diameter (EQD), defined as the diameter of a circle with the same area as that of the measured pit shape, is reported.

To normalize the data per unit area, we assumed that the area observed was $9.2 \cdot 10^{-9} \text{m}^2$ (one-half the surface area of particles of diameter 53 to 100 μm , assuming spherical geometry). To obtain PSDs, we calculated the cumulative pit size distribution function, $N(W)$, and calculated the value of $n(W)$ for each pit size as the slope of N with respect to W , $(N_{i+1} - N_i)/(W_{i+1} - W_i)$ (Cashman and Ferry, 1988). Regressions of $\ln(n)$ vs. W for each data set yielded the slope ($= -1/G\tau$) and the intercept, $\ln(n^0)$ (Table 2).

Results

Examination of the soil samples under SEM using EDX revealed that grains identified as pyriboles by Creameens et al. (1992) were ferrohornblende in composition ($\text{Ca}_2(\text{Fe} > \text{Mg})_5 \text{Si}_7 \text{AlO}_{22}(\text{OH})_2$). Etch pits on these grains show a characteristic lens shape, while etch pits on potassium feldspar reveal more equant shapes (Figure 1). In most of the PSD plots, the number of smallest and largest pits do not fall exactly on a linear trend for each horizon (Figure 2). Nonlinearity is most apparent in the poorly-drained soil. In each case, we have fitted a line to the linear part of the curve (asterisks in Table 1 indicate data not used for the regressions).

Table 2 reveals little variation in the PSD constants (slope and intercept) with soil horizon within each soil. Within 95% confidence, the upper two horizons of each soil show the same value of n^0 and $G\tau$ for both minerals. Calculation of n^0 and $G\tau$ for each mineral in each soil regressed over the top two soil horizons (Table 2, Figure 2) reveals that n^0 increases and $G\tau$ decreases for both potassium feldspar and hornblende from well- to somewhat-poorly to poorly-drained soils.

Discussion

For all cases, exactly linear PSDs were not observed. The lack of small pits might be due to the limits of resolution (e.g. Figure 2b, 2d, 2f). An overabundance of large etch pits is also observed in some samples. Assuming that an overabundance of large pits suggests pit coalescence, coalescence occurred most significantly in the samples from the poorly drained soil (Traer, Fig. 2e, f).

Table 2. PSD coefficients and etch rates ($\pm 1\sigma$)

Soil	Horizon	Depth (cm)	Number of pits	$\log n^\circ$	$G\tau$ ($\times 10^{-7}$) (m)	G (min) ($\times 10^{18}$) (m/s)	J (min) ($\#/m^2s$)	R_{pit} ($\times 10^{-15}$) (mol/ m^2s)
<i>potassium feldspar</i>								
Fayette (well-drained)	BE	20-31	3448	18.17 \pm 0.10	5.23 \pm 0.25			2.6 \pm 1.3
	Bt	31-69	2955	18.26 \pm 0.10	4.88 \pm 0.22			2.4 \pm 1.1
	C	205-220	1413	17.78 \pm 0.07	5.50 \pm 0.21			1.3 \pm 0.5
	BE, Bt	20-69		18.21 \pm 0.08	5.05 \pm 0.18	1.29	2.1	2.5 \pm 1.0
Stronghurst (s. po. drained)	E	18-32	4415	18.41 \pm 0.08	4.43 \pm 0.13			2.3 \pm 0.8
	Bt	48-68	4426	18.47 \pm 0.10	4.34 \pm 0.17			2.4 \pm 1.1
	Cg	165-242	2608	18.10 \pm 0.04	4.99 \pm 0.06			1.8 \pm 0.3
	E, Bt	18-68		18.44 \pm 0.06	4.39 \pm 0.09	1.12	3.1	2.4 \pm 0.6
Traer (poorly drained)	E	26-37	5440	18.72 \pm 0.08	3.56 \pm 0.12			2.0 \pm 0.8
	Btg	37-73	7425	18.65 \pm 0.06	4.06 \pm 0.11			2.8 \pm 0.8
	Cg	165-242	3750	18.51 \pm 0.12	4.06 \pm 0.19			2.0 \pm 1.1
	E, Btg	26-73		18.68 \pm 0.09	3.78 \pm 0.13	0.96	4.6	2.3 \pm 0.9
<i>hornblende</i>								
Fayette (well-drained)	BE	20-31	4495	18.31 \pm 0.09	7.36 \pm 0.37			9.0 \pm 3.9
	Bt	31-69	5650	18.27 \pm 0.04	7.62 \pm 0.27			9.4 \pm 2.6
	C	205-220	4197	18.04 \pm 0.07	8.52 \pm 0.33			8.7 \pm 3.2
	BE, Bt	20-69		18.29 \pm 0.05	7.49 \pm 0.26	1.91	3.7	9.2 \pm 2.8
Stronghurst (s. po. drained)	E	18-32	5400	18.46 \pm 0.10	6.12 \pm 0.26			6.1 \pm 2.9
	Bt	48-68	4730	18.38 \pm 0.06	6.68 \pm 0.20			7.2 \pm 2.2
	Cg	165-242	3560	18.36 \pm 0.09	6.03 \pm 0.25			4.6 \pm 2.0
	E, Bt	18-68		18.42 \pm 0.06	6.39 \pm 0.19	1.63	4.3	6.6 \pm 2.0
Traer (poorly drained)	E	26-37	7466	18.52 \pm 0.06	5.79 \pm 0.31			5.6 \pm 2.2
	Btg	37-73	7766	18.77 \pm 0.10	5.05 \pm 0.18			5.8 \pm 2.6
	Cg	180-242	6978	18.62 \pm 0.08	5.43 \pm 0.20			5.4 \pm 2.1
	E, Btg	26-73		18.60 \pm 0.06	5.57 \pm 0.21	1.42	5.6	5.8 \pm 1.0

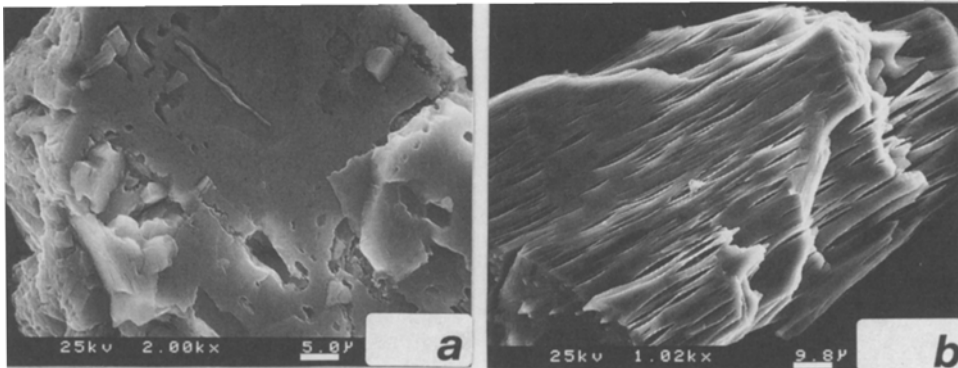


Figure 1. SEM photomicrographs of (a) potassium feldspar grain from Bt horizon of the Stronghurst soil; (b) hornblende grain from the Bt horizon of the Fayette soil. Scale bar is indicated at the bottom of each photograph.

For several cases, coefficients in the *C* horizon differ from the other two horizons (to 95% confidence). We conclude that the upper two horizons of all the soils have reached steady state and coefficients are equal within the error of the estimate, but that the PSDs in the *C* horizon of each soil may or may not have reached steady state. Difference between soils in coefficients for the *C* horizons suggest that PSDs indicate modern, rather than inherited weathering. The *C* horizon PSDs may therefore indicate a difference in the extent of weathering.

Samples show an increase in nucleation density, n^0 (regressed over the top two horizons), with decreasing drainage. As drainage decreases, soil grains remain wetted, or partially wetted, for longer intervals. This implies that the average wetted surface area of grains increases with decreasing drainage, explaining the increased nucleation density, n^0 .

Assuming that τ = total etching period (12,500 y), then growth rate, G , and nucleation rate, J , can be calculated for each profile (Table 2). However, because τ (mean pit lifetime) must be less than or equal to the total etching time because of annihilation, this value of G and J represents a minimum. Calculated minimum growth (G) and nucleation rates (J) for potassium feldspar and hornblende show a slight decrease (G) and increase (J) with decreasing drainage. Brantley et al. (1986) observed that nucleation rates for etch pits on hydrothermally etched quartz decreased gradually with increasing saturation index, but that, above the critical saturation, nucleation rate went to 0. It follows that soil pore waters in the catena are undersaturated and do not approach C_{crit} . The observed decrease in G with decreasing drainage may be correlated with differences in pore water chemistry as drainage decreases. If porewaters have higher saturation indices or inhibitor concentrations due to poor drainage, these parameters might explain the observed decrease in calculated growth rate, G .

Recognizing that $G = 2v_x$, we can use Equation (5) to estimate the rate of dissolution due to etch pit nucleation and growth (Table 2). Because no measurements of etch pit geometry are available, we follow MacInnis and Brantley (1993) and model pits as right pyramids ($\theta = 45^\circ$, $V(\text{orthoclase}) = 1.09 \cdot 10^{-4} \text{ m}^3/\text{mol}$, $V(\text{hornblende}) = 1.69 \cdot 10^{-4} \text{ m}^3/\text{mol}$), using W = the equivalent diameter. The assumption of a regular pit geometry is

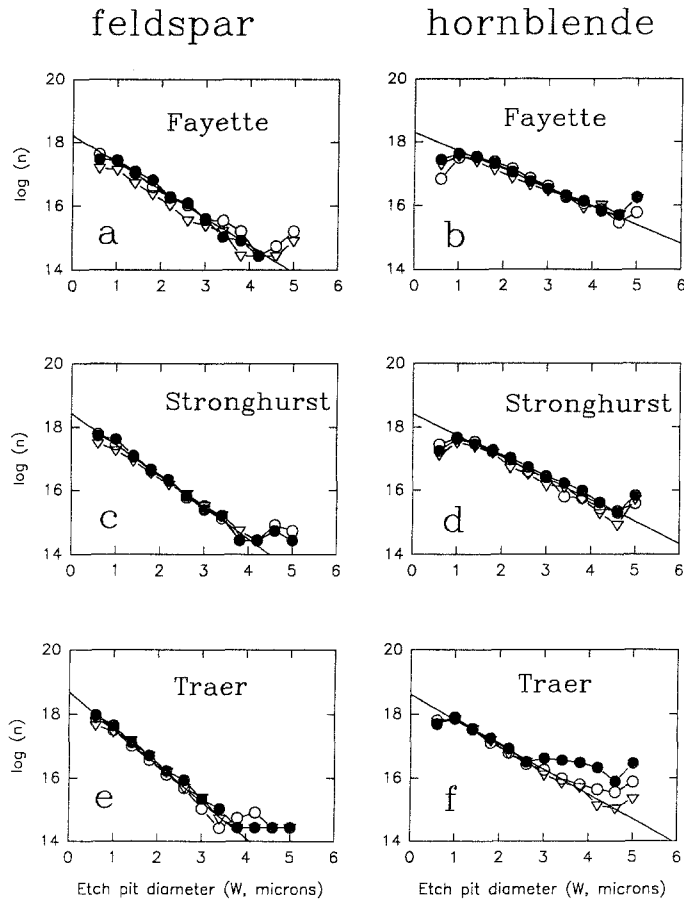


Figure 2. PSD plots for three horizons of three soils. Dotted line in every case represents regression of data for each soil for the top two horizons (data points not included in the regressions are noted in Table 1). Abscissa represents etch pit size in microns; ordinate represents $\log_{10} n$, where n is number of pits per size range per m^2 area. (a) Fayette (well-drained) soil, potassium feldspar; (b) Fayette soil, hornblende; (c) Stronghurst (somewhat poorly drained) soil, potassium feldspar; (d) Stronghurst soil, hornblende; (e) Traer (poorly drained) soil, potassium feldspar; (f) Traer soil, hornblende. In every diagram, the open circle is the uppermost soil horizon, the solid circle is the middle horizon, and the triangle is the lowermost horizon (see Table 2 for horizon designations).

more acceptable for hornblende than for potassium feldspar (Figure 1). Etch pits in hornblende are roughly as deep as they are wide (average width for 137 grains from Bt horizon of the Fayette soil was $0.91 \pm 0.28 \mu m$); in contrast, etch pits on potassium feldspar show no such characteristic dimensions, and sometimes occur as very deep features. For this reason, etch pit dissolution rates calculated for hornblende should be more accurate than those for potassium feldspar.

For every soil, etching rate is lowest in the C horizon, although large error bars obscure the interpretation. The number of etch pits observed on soil grains from the C horizon was always the lowest. The greatest etching rate was observed in the upper B horizon of

almost every soil. In this horizon, the pH is at a minimum. The etching rates for hornblende calculated here were slightly faster than rates estimated from one soil grain in our previous work, $0.27 - 2.3 \cdot 10^{-15}$ mol/m² s (MacInnis and Brantley, 1993); rates for feldspar dissolution matched our earlier work, $2.4 - 2.3 \cdot 10^{-15}$ mol/m² s.

Equation 5 shows that R_{pit} is a function of n° and G^4 ; the fact that n° increases and G decreases with decreasing drainage suggests that the net effect of decreasing drainage might be to decrease R_{pit} . However, comparison of pit dissolution rates between soils indicates that potassium feldspar dissolution is independent of drainage, within the error of the measurement. Cremeens et al. (1992) also noted that resistate maturity and the quartz/feldspar ratios were consistent for similar depths between the profiles, indicating the relative degree of weathering of the soils – based on felsic minerals – is the same. In contrast, etch rate of hornblende appears to decrease with decreasing drainage (Table 2). A similar conclusion was reached by Cremeens et al. (1992) based on pit size frequency distribution.

For every soil, potassium feldspar etch rates are lower than hornblende etch rates, as predicted by most weathering sequence compilations (e.g. Velbel, 1993). In all cases, etching rates are lower than laboratory dissolution rates, as expected given that laboratory rates include dissolution at all sites, not just etch pits, on the surface: potassium feldspar dissolves at a rate of $173 \cdot 10^{-15}$ mol/m² s (Schweda, 1990) and hornblende dissolves at a rate of $1820 \cdot 10^{-15}$ mol/m² s (Nickel, 1973) or $4200 - 8300 \cdot 10^{-15}$ mol/m² s (Sverdrup, 1990) in the laboratory. The ratio of hornblende/potassium feldspar dissolution rate (2–4) is smaller for etching estimates than for laboratory dissolution (10–50). If we assume that our assessment of pit geometry was adequate, then we conclude that either (i) pit dissolution as a contributor to total dissolution rate varies between potassium feldspar and hornblende; or (ii) factors slowing dissolution in the field affect hornblende and potassium feldspar differently. If (ii) is correct, then we disagree with Velbel (1993); chemical rather than physical factors may explain the laboratory-field discrepancy. The observation that dissolution of hornblende was slower in the poorly drained soil where grain wetting was extensive suggests that, for that phase, chemical factors may explain the low rates of weathering observed in natural systems.

Conclusions

Application of the pit size distribution model to etch pits developed on potassium feldspar and hornblende grains from a loess soil reveals that pit sizes show a power-law distribution as predicted by the model, although a superabundance of large pits for most distributions may be caused by coalescence. The PSD model yields a quantitative estimate of weathering rates. The irregular geometry of the potassium feldspar pits introduces more uncertainty into the dissolution estimate for the phase. Laboratory quantification of etch pit growth rates of each mineral would allow modelling of precise pit geometries, which would yield more accurate assessments of mineral dissolution. Analysis of PSDs for other young soil profiles – especially for soils where grains do not show inherited weathering features – should reveal patterns of weathering rates for soil horizons and types.

The etching data suggests that soil pore waters did not reach the critical saturation value where nucleation of etch pits on feldspar and hornblende terminates. This is in contrast with observations from quartz grains pitted in a tropical environment (Brantley et al.,

1986). Growth rates of pits decrease with decreasing drainage, suggesting that, as the pore water moves closer to saturation or as inhibitor concentrations increase, pit growth decreases. Decreasing drainage also correlates with an increase in pit nucleation density; this increase offsets the decreased pit growth rate. The PSD model predicts that etching is a stronger function of growth rate (and thus solute concentration), than nucleation density (and thus wetting). Etching rate of hornblende as a function of drainage in a loess soil shows that increased solute concentrations slowed the rate more than increased wetting; in contrast, etching rate of potassium feldspar showed no variation with drainage.

ACKNOWLEDGEMENT

We are honored to participate in this volume dedicated to P. Schindler, especially at this point in the development of both surface adsorption and surface-controlled dissolution models for minerals. Schindler's contributions laid the groundwork for the synthesis of surface spectroscopic data, adsorption data, and kinetic data which is presently occurring. S.L.B. acknowledges funding from N. S.F. grant EAR-8657868 and the David and Lucile Packard Foundation. We acknowledge contributions from L. D. Norton, D. Voigt, P. Richards, L. Kump and C. Perry.

REFERENCES

- Bouma, J., 1983. Hydrology and soil genesis of soils with aquic moisture regimes. In: L. F. Wilding, N. E. Smeck and G. F. Hall (eds.), *Pedogenesis and Soil Taxonomy*, Elsevier, New York: pp. 253–281.
- Brantley, S. L., S. R. Crane, D. A. Crerar, R. Hellmann and R. Stallard, 1986. Dissolution at dislocation etch pits in quartz. *Geochim. Cosmochim. Acta* 50:2349–2361.
- Brantley, S. L., 1992. Kinetics of dissolution and precipitation – Experimental and field results. In: Y. Kharaka and A. S. Maest (eds.), *Balkema, Amsterdam: 7th International Symposium on Water-Rock Interaction*, pp. 3–6.
- Cashman, K. V. and J. M. Ferry, 1988. Crystal size distribution (CSD) in rocks and the kinetics and dynamics of crystallization, III. Metamorphic crystallization. *Contrib. Mineral. Petrol.* 99:401–415.
- Claasen, H. C. and A. F. White, 1979. Application of geochemical data to ground-water systems – a tuffaceous rock system in southern Nevada. In: E. A. Jenne (ed.), *Chemical Modeling in Aqueous Systems*, Am. Chem. Soc. Washington, D. C.: pp. 771–793.
- Creameens, D. L., R. G. Darmody and L. D. Norton, 1992. Etch-pit size and shape distribution on orthoclase and pyriboles in a loess catena. *Geochim. Cosmochim. Acta* 56:3423–3434.
- Hall, R. D. and L. L. Horn, 1993. Hornblende etching in soils in glacial deposits of the northern Rocky Mountains. *Chemical Geology* 105:17–30.
- Kerrick, D. M., A. C. Lasaga and S. P. Raeburn, 1991. Kinetics of heterogeneous reactions In: D. M. Kerrick (ed.), *Rev. Mineral.* 26, Mineral. Soc. America: *Contact Metamorphism*, pp. 583–671.
- MacInnis, I. N. and S. L. Brantley, 1993. Development of etch pit size distributions on dissolving minerals. *Chemical Geology* 105:31–49.
- Nickel, E., 1973. Experimental dissolution of light and heavy minerals in comparison with weathering and intracrystalline dissolution. *Contrib. Sediment.* 1:1–68.
- Paces T., 1983. Rate constants of dissolution derived from the measurements of mass balance in hydrological catchments. *Geochim. Cosmochim. Acta* 37:1855–1863.
- Rowe, G. L. and S. L. Brantley, 1993. Estimation of the dissolution rates of andesitic glass, plagioclase and pyroxene in a flank aquifer of Poas Volcano, Costa Rica. *Chemical Geology* 105:71–88.
- Schindler, P. W. and W. Stumm, 1992. The surface chemistry of oxides, and oxide minerals. In: W. Stumm, (ed.), *Coordination Chemistry of the Oxide-Water Interface*. John Wiley and Sons, New York.
- Schweda, P., 1990. Kinetics and mechanisms of alkali feldspar dissolution at low temperatures. Ph.D. Dissertation, Department of Geology and Geochemistry, Stockholm University, Stockholm, unpublished.

- Sverdrup, H., 1990. The kinetics of base cation release due to chemical weathering. Lund University Press, Lund, 246 pp.
- Swoboda-Colberg, N. and J.I. Drever, 1993. Mineral dissolution rates in plot-scale field and laboratory experiments. *Chemical Geology* 105:51–70.
- Velbel, M.A., 1993. Constancy of silicate-mineral weathering-rate ratios between natural and experimental weathering: implications for hydrologic control of differences in absolute rates. *Chemical Geology* 105:89–100.

Received 2 July 1993;
manuscript accepted 6 September 1993.